Heliyon 5 (2019) e02636

Contents lists available at ScienceDirect

Heliyon

journal homepage: www.heliyon.com

Heliyon

Research Article

Revealing the ultrastructure of the membrane pores of intact *Serratia marcescens* cells by atomic force microscopy

Yu-Chun Lin [a,*], Cheng Huang [a,b], Hsin-Chih Lai [c]

[a] Department of Biotechnology and Laboratory Science in Medicine, National Yang-Ming University, Taipei, 11221, Taiwan
[b] Department of Earth and Life Sciences, University of Taipei, Taipei, 11153, Taiwan
[c] Department of Biotechnology and Laboratory Science, Chang Gung University, Taoyuan City, 33302, Taiwan

ARTICLE INFO

Keywords:
Microbiology
Cell biology
Biomedical engineering
Biomechanics
Cell biology
Microbiology
Medical imaging
Serratia marcescens
Atomic force microscopy
Surface membrane pore
Transmembrane subunit channel

ABSTRACT

This study aimed to characterize the surface ultrastructure of intact *Serratia marcescens* cells under physiological conditions. Topographic information of membrane pores of the cells was obtained by atomic force microscope (AFM). Three types of membrane pores (CH-1-*Pore A*, CH-1-*Pore B* and CH-1-*Pore C*) were observed and the spatial arrangements of membrane-spanning subunits in membranes were defined. High-resolution images revealed that the doughnut-shaped structures of CH-1-*Pore A* and CH-1-*Pore B* were composed of six-to-eight and four transmembrane subunits. The inverted teepee-shaped structure of CH-1-*Pore C* was segmented into two transmembrane subunits straddling a single funnel-like pore. This study, to the best of authors' knowledge, represents the first direct characterization of the surface ultrastructure of the membrane pores of *Serratia marcescens* CH-1 cells at the nanometer scale and offers new prospects of mapping membrane pores on intact prokaryotic cells.

1. Introduction

Multidrug-resistant bacterial infections have become risks to global health [1]. *Serratia marcescens* (*S. marcescens*) is a Gram-negative bacillus and an important nosocomial pathogen that causes various infections [2]. Gaining insights into the physicochemical and structure of the cells, especially the membrane pores, may help with understanding the pathogenesis of *S. marcescens*. The atomic force microscope (AFM) [3] has recently attracted the interests of cell and membrane biologists [4]. This new approach could provide topological information on the images of both cell surface and membrane structures at a significantly higher resolution than the optical microscope in aqueous medium [5]. Traditional optical microscopes are limited by diffraction owing to the nature of light wave. In contrast, AFM can achieve molecular and atomic resolution on many materials [6, 7, 8, 9]. In addition, three-dimensional information can be extracted directly from AFM topographic and phase images.

Several classes of membrane pores have been discovered in prokaryotic cells [10]. Rem *et al.* discovered the pore-forming subunits of a sodium channel [11]. Armstrong *et al.* reported an ionotropic glutamate receptor [12]. Several groups measured the cell membrane electro-physiologically, and described classes of voltage-gated, inward rectifier and calcium-activated potassium channels [13, 14, 15]. ClC-type chloride channels [16, 17, 18] have also been observed. Although various prokaryotic membrane channels were described in the literatures, relatively little is known about their spatial arrangements and three-dimensional topographies. Membrane channels have been reported to be in the mesoscopic scale of 1–100 nm (10–1000 Å) [19, 20]. In this work, we demonstrated that AFM can be employed to investigate the ultra structure of each single membrane pore of intact *S. marcescens* CH-1 cell, which is currently inaccessible by conventional microscopic. By using AFM, we better defined the structural arrangement of transmembrane structures on integral membranes than on isolated membrane. This work provides a feasible approach to investigate the relationship of three-dimensional membrane pore structures and functions on living prokaryotic cells.

* Corresponding author.
E-mail address: ylinz@umich.edu (Y.-C. Lin).

https://doi.org/10.1016/j.heliyon.2019.e02636
Received 16 August 2019; Received in revised form 19 September 2019; Accepted 8 October 2019

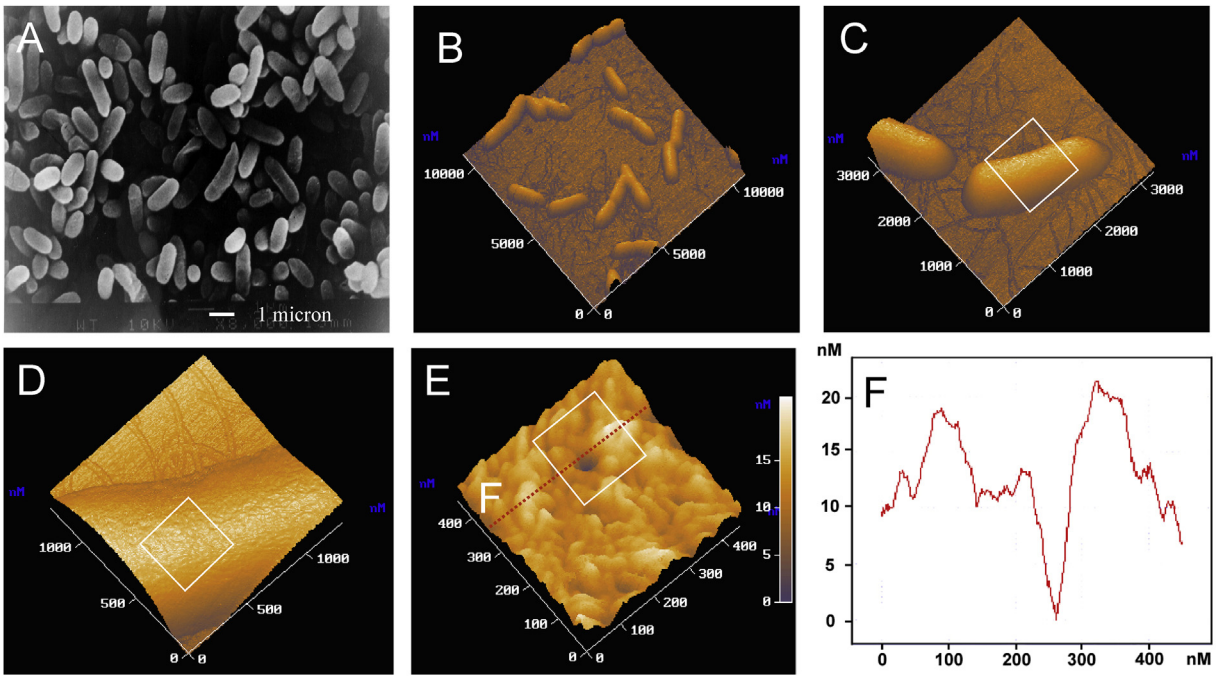

Fig. 1. (A) An SEM image of the *S. marcescens* CH-1 cells. (B–E) Three-dimensional AFM topographic images of the *S. marcescens* CH-1 cells adsorbed on poly-L-lysine-coated mica. The AFM scanning areas are 10 × 10 (B), 3 × 3 (C), 1.5 × 1.5 (D), and 0.5 × 0.5 (E) μm^2 for the low- and higher-resolution images, respectively. Images acquired by zooming into the boxed areas of Fig. 1B, C and D are displayed in Fig. 1C, D and E, respectively. The higher-resolution image (E) shows that many protrusions like mountain ranges and hills exist on the surface and (F) the corresponding cursor profile reveals the presence of an individual membrane pore.

2. Materials and method

2.1. Cell preparation

Stock cultures of *S. marcescens* CH-1 were maintained at -80 °C. *S. marcescens* CH-1 used in this work was grown to mid-log phase in Terrific Broth (Difco Laboratories; 10 mL) at 37 °C for 7 hours in the presence of 50 μg/mL kanamycin A. Bacterial concentrations were determined by measuring the absorbance of the culture at 600 nm ($0.1 \times O.D._{600} = 10^8$ cells/mL) in a spectrophotometer (Jasco V-550 UV-VIS spectrophotometer). The final bacterial concentration is approximately $(5–9) \times 10^9$ cells/mL. Before the experiment, the bacteria culture was centrifuged at 2050 × *g* (4510 rpm) for 5 min at 4 °C. The wet pellet was then re-suspended in distilled water, and recentrifuged (2x) to remove the growth medium. Final pellet was suspended in PBS solution. A drop of 0.01 % (wt/vol) poly-L-lysine hydrobromide solution (a positively charged compound), was added on to the mica and incubated for 30 min followed by washing with Milli-Q water before the introduction of the specimens. After washing once with PBS, the *S. marcescens* CH-1 cells were then placed in contact with the mica that had been coated with poly-L-lysine hydrobromide. *S. marcescens* CH-1 cells were attached to the mica through electrostatic interactions (physical adsorption).

2.2. Atomic force microscopy and scanning electron microscopy analysis

AFM experiments were carried out with a Smena B™ AFM (NT-MDT, Moscow) in tapping mode. Light tapping was used, which involved maintaining a high amplitude set point relative to the free amplitude of the cantilever. We used silicon cantilevers Ultrasharp™ NSG11 (Mikro-Masch, Estonia) with a spring constant of 0.06 N/m. The oscillation amplitude was 50–100 nm with set point ratio of 0.9. Images were collected in a narrow range of frequencies (120–130 kHz). In general, we began by scanning an area of 10 μm × 10 μm that covered several bacteria cells. Image size was later reduced to isolate individual cells. To avoid the image alteration by the tip artifacts, such as hysteresis, we scanned the cells in x and y directions several times before capturing an image. Three to six high-quality images were captured from each preparation, and one image among these was selected for three-dimensional presentation. Tips were replaced frequently, or when there was any indication of artifacts present in the images.

For scanning electron microscopy (SEM), *S. marcescens* CH-1 cells were fixed with 2.5% glutaraldehyde. Samples were then critical-point dried with CO_2 and coated with gold (S150 sputter coater). Cells were observed with an SEM (Hitachi S-3500N) operating at an accelerating voltage of 20 kV.

2.3. Data analysis

After images were recorded, an offline section analysis was performed on each image in order to gain information on sample topography. A line was drawn across the image, and the topography of the sample as a function of distance was displayed. The height traces were performed to provide more information on each membrane pore (conducted according to the manufacturer's software program). The difference between maximum and minimal values of the z coordinate on the surface within the area (height drop) was defined as "valley to peak" value (R_{max}): $R_{max} = z_{max} - z_{min}$. The average value of the z coordinate on the sample surface was defined as "mean height" value (R_{mean}): $R_{mean} = Z_{mean} = \frac{1}{N_x N_y}\sum_{i=1}^{N_x}\sum_{j=1}^{N_y} Z_{ij}$, $z = z_{ij} - R_{mean}$, where N represents the sample number. The mean height is the sum of the sampled values divided by the number of items in the sample. The average value of the surface roughness within the area being analyzed is defined as "surface roughness" value (R_a): $R_a = \frac{1}{N_x N_y}\sum_{i=1}^{N_x}\sum_{j=1}^{N_y}|z(i,j) - z_{mean}|$, $Z_{mean} = \frac{1}{N_x N_y}\sum_{i=1}^{N_x}\sum_{j=1}^{N_y} Z_{ij}$, in which each reference point was compared with the mean Z value, and the sum of the values was divided by the number of items. The surface "root-mean-square" value (R_q) was calculated as the standard deviation of z coordinate on the sample surface within the area: $R_q = \sqrt{\frac{1}{N_x N_y}\sum_{i=1}^{N_x}\sum_{j=1}^{N_y}(z(i,j) - z_{mean})^2}$, where the value is the square root of the arithmetic mean of the squares of the values.

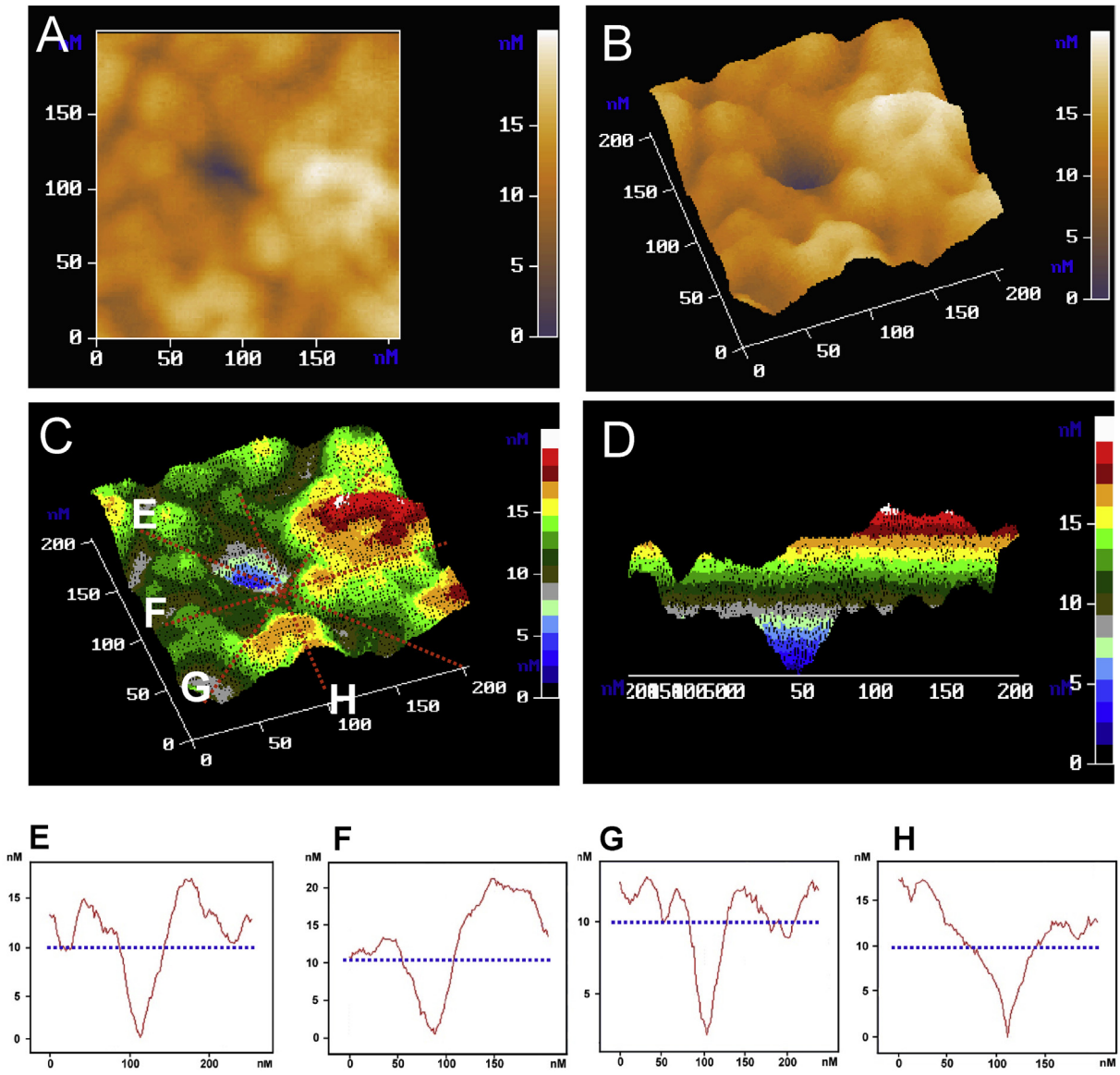

Fig. 2. Exemplary imaging of the first type of membrane pore CH-1-*Pore A* observed with AFM. (A) and (B) Two- and three-dimensional top view of an individual pore in the outer membrane of *S. Maccensis* from the extracellular side. (C) A contour view of Fig. 2B. (D) View from within the membrane with the extracellular region above and the intracellular region below. (E–H) (depicted from red lines in Fig. 2C). Profiles of the internal canal indicating the measurable inner diameters. The doughnut-like structure displayed in Fig. 2B is segmented into six to eight subunits. The blue dot line indicates the approximately surface height (R_{mean} = 9.95 nM) of the outer membrane.

3. Results

3.1. The topological information of the surface and membrane structure of *S. marcescens* CH-1 cells

The detailed surface topography of *S. marcescens* CH-1 was studied using AFM and SEM (Fig. 1). Fig. 1A shows the images of the *S. marcescens* CH-1 cells captured by scanning electronic microscopy. SEM images demonstrate that the cells were in rod shape with lateral dimensions of about 0.5 and 2 microns. Fig. 1B shows the AFM topographic image of *S. marcescens* CH-1 cells that were attached to poly-L-lysine-coated mica through physical adsorption. Fig. 1C represents one single rod-shaped cell that was acquired by zooming into the boxed area in Fig. 1B. The quantitative measurement of the dimensions of the cells revealed that the length and width of CH-1 were 2028 nm and 798 nm, respectively. The findings were similar to the ones that were obtained by thin-section electronic microscopy [21]. We measured over thirty of cells, and found the root means square (RMS) values of *S. marcescens* CH-1 were of 1996 ± 68 nm in length and 804 ± 47 nm in width. Although some variations existed in the exact sizes of surface features, the traces were reproducible. We then reduced area of interest size and zoomed into specific areas to scan individual cell surface (boxed areas in Fig. 1C and D). Exemplary AFM image (Fig. 1E) showed that many protrusions-like mountain ranges and hills existed on the surface of cell. Height trace of the line in Fig. 1E is shown in Fig. 1F; the corresponding cursor profile revealed the presence of an individual membrane pore.

3.2. Ultrastructure of CH-1-Pore A

To investigate the detailed surface topography of the membrane pore, higher-resolution two- (Fig. 2A) and three-dimensional (Fig. 2B) images were obtained by zooming into the boxed area in Fig. 1E (scanning area 200 × 200 nm^2). Fig. 2C shows the contour view of the three-dimensional image (Fig. 2B). Fig. 2D illustrates the side view from

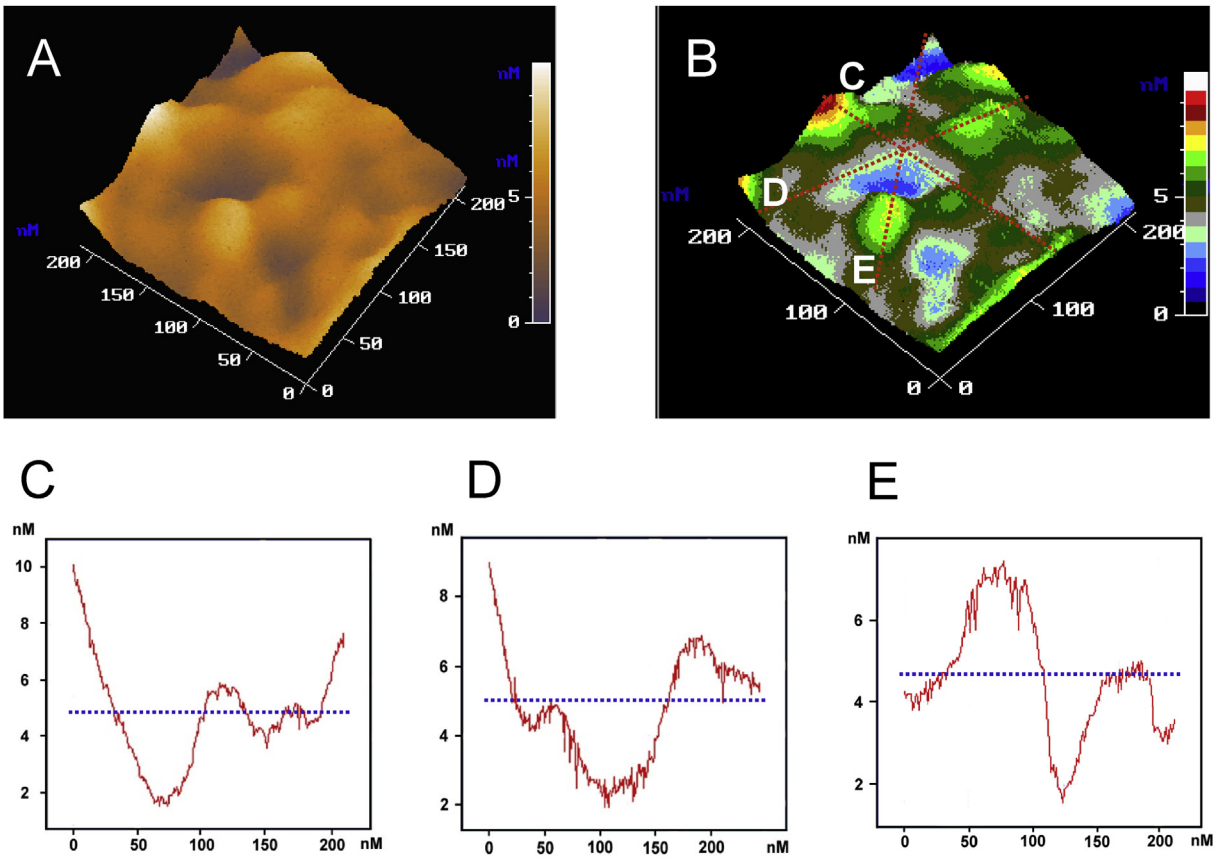

Fig. 3. Exemplary imaging of the second type of membrane pore CH-1-*Pore B*. (A) Three-dimensional top view of an individual pore in the outer membrane of *S. Maccensis* from the extracellular side. (B) A contour view of B. (C–E) (red lines in B) Profiles of the internal canal indicating the measurable inner diameters. The doughnut-like structure is apparently segmented into four subunits. The blue dot line indicates the approximately surface height (R_{mean} = 4.72 nM) of the outer membrane.

within the membrane with the extracellular region above and the intracellular region below. These high-resolution images revealed the presence of a funnel-like membrane pore with distinguishable surface protrusions that surrounded the pore (Fig. 2B and C). Height trace of the lines in Fig. 2C is shown in Fig. 2E, F, G and H. The doughnut-shaped structure appears to be composed of six to eight membrane-spanning subunits and a single funnel-like pore (CH-1-*Pore A*) with a lateral diameter of 56.0 × 65.6 nm with 13.4–21.7 nm above the membrane plane (Fig. 2E, F, G, H). These results resembled the AFM image of the membrane pores of isolated nuclei from Jurkat and FL5 cells [22]. The funnel-like profile of the opening of the pore (Fig. 2H) shows that the pore had a wide vestibule that was more constricted towards the lipid bilayer.

3.3. Ultrastructure of CH-1-Pore B

We then examined over 30 of *S. marcescens* CH-1 cells in detail to obtain more information of the membrane pores. Although we noted some variations exist in the dimensions of these cells, we observed the presence of two more different types of outer membrane pores on intact *S. marcescens* CH-1 cells' surfaces. Fig. 3A shows the exemplary image of the second type of membrane pore (CH-1-*Pore B*) that presented on the outer membrane. A contour view of Fig. 3A is displayed in Fig. 3B. Height trace of the lines in Fig. 3B revealed the profile of the pore (Fig. 3C, D, E). The finding demonstrated that the doughnut-shaped structure appeared to be composed of four membrane-spanning subunits and a single funnel-like pore. The lateral dimensions of this type of pore were 57.5 × 70.2 nm that raised 4.1–10.2 nm above the membrane plane.

3.4. Ultrastructure of CH-1-Pore C

A third type of membrane pore (CH-1-*Pore C*) was also observed. Fig. 4A shows the exemplary image of an individual pore that was observed on the outer membrane. Fig. 4B displays the contour view of Fig. 4A, which shows inverted teepee-shaped structure segmented into two membrane-spanning subunits straddling a single funnel-like pore. AFM analysis demonstrated that pore diameter was 77.9 × 128.3 nm and the pore raised 9.0–12.8 nm above the membrane plane (Fig. 4C, D, height trace of the lines in Fig. 4B).

3.5. Analysis of different pores

The surface topographies of three different types of membrane pores that were depicted in Fig. 2 (CH-1-*Pore A*), 3 (CH-1-*Pore B*) and 4 (CH-1-*Pore C*) were then systematically studied. Over six of each type of membrane pores were examined. The surface traces were reproducible for each type of membrane pore, despite some variations in the pore diameter and height of transmembrane subunit at each membrane pore.

Table 1 lists surface properties of the three types of membrane pores: CH-1-*Pore A*, CH-1-*Pore B*, and CH-1-*Pore C* that were observed on the *S. marcescens* CH-1 cell in this study. We found that CH-1-*Pore A* had the highest mean height (R_{mean}) among the three (8.65 ± 1.92 nm), with the longest peak-to-peak distance (R_{max}) of 19.79 ± 2.88 nm, and a surface roughness (R_a) of 1.79 ± 0.32 nm. CH-1-*Pore B* had R_{mean} of 4.72 ± 0.65 nm, R_{max} of 9.20 ± 1.78 nm, and R_a of 0.99 ± 0.11 nm. CH-1-*Pore C* had R_{mean} of 6.22 ± 0.83 nm, R_{max} of 11.75 ± 1.03 nm, and R_a of 0.98 ± 0.17 nm. In addition, CH-1-*Pore A* was found to have six to eight transmembrane subunits; while CH-1-*Pore B* and CH-1-*Pore C* were found to

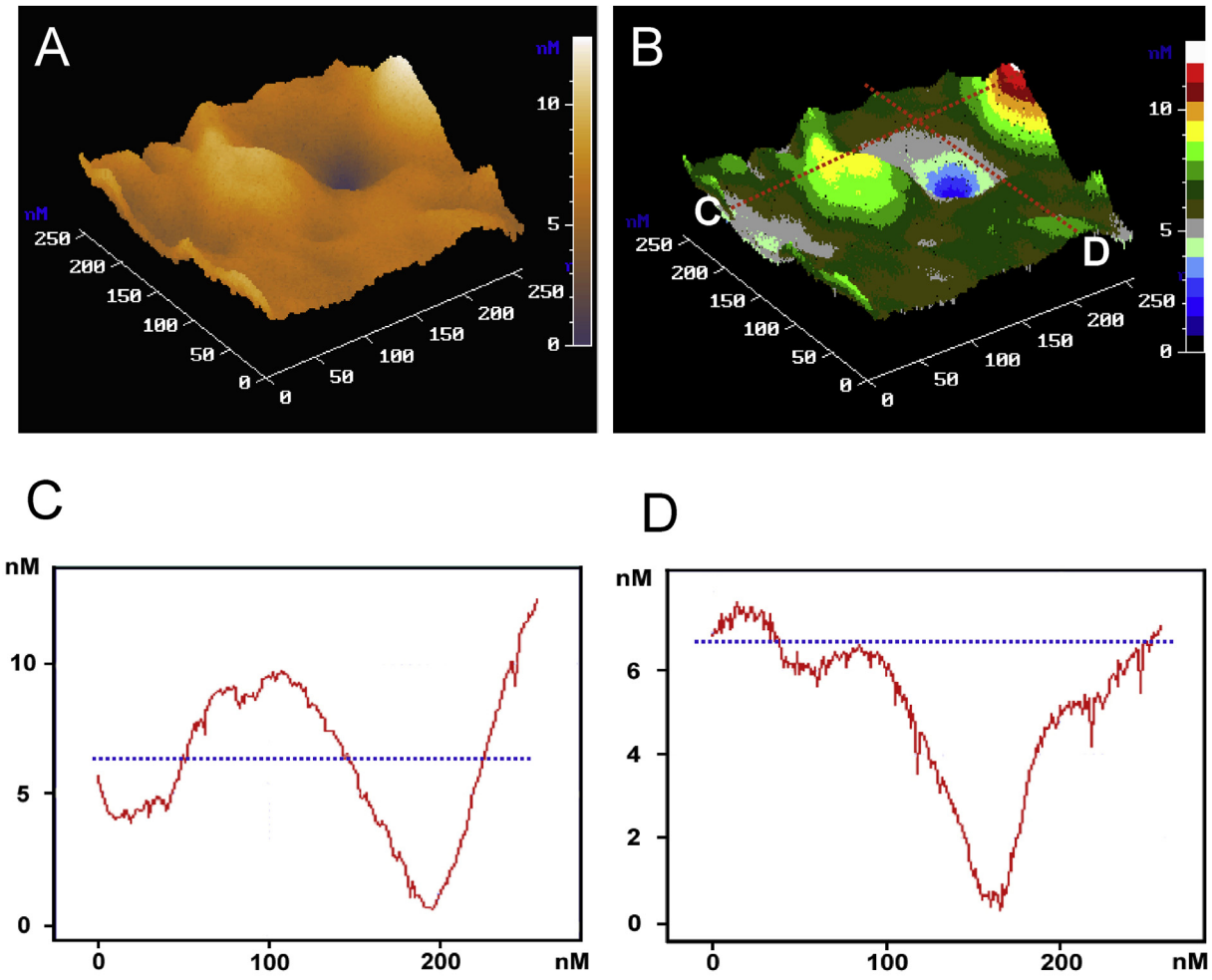

Fig. 4. Exemplary AFM imaging of the third type of membrane pore CH-1-*Pore C*. (A) Three-dimensional top view of an individual pore in the outer membrane of *S. Maccensis* from the extracellular side. (B) A contour view of B. (C–D) (see red lines in B) Profiles of the internal canal indicating the measurable inner diameters. The inverted teepee-shaped structure is apparently segmented into two subunits. The blue dot line indicates the approximately surface height (R_{mean} = 6.23 nM) of the outer membrane.

Table 1
The topographic properties of three different types of membrane pores displayed in Fig. 2 (CH-1-*Pore A*), Fig. 3 (CH-1-*Pore B*) and Fig. 4 (CH-1-*Pore C*).

	CH-1-*Pore A*	CH-1-*Pore B*	CH-1-*Pore C*
Example	Fig. 2	Fig. 3	Fig. 4
Peak-to-peak distance (nm)	19.79 ± 2.88	9.20 ± 1.78	11.75 ± 1.03
Roughness (nm)	1.79 ± 0.32	0.99 ± 0.11	0.98 ± 0.17
Mean height (nm)	8.65 ± 1.42	4.72 ± 0.65	6.22 ± 0.83
Root-mean-square (nm)	2.32 ± 0.22	1.28 ± 0.21	1.42 ± 0.28
Pore diameter (nm)	(54.03 ± 3.79) × (66.62 ± 4.72)	(56.14 ± 3.05) × (69.26 ± 4.71)	(78.50 ± 5.79) × (120.37 ± 10.48)
transmembrane subunit	six – eight	four	two
Height of transmembrane subunit (nm)	(13.41 ± 2.79) – (19.79 ± 2.88)	(3.92 ± 0.59) – (11.16 ± 1.59)	(8.52 ± 0.89) – (12.97 ± 0.59)

have four and two transmembrane subunits surrounding a central pore, respectively.

4. Discussion

In this study, we revealed the first time the surface structure of intact *S. marcescens* CH-1 cells. We showed that AFM is a valuable tool to provide surface information on integral prokaryotic bacteria. By probing the surface of individual *S. marcescens* CH-1 cell with AFM, we discriminated three different types of transmembrane pores. These pores were then visualized and measured, and the surface topographic profile of each pore was depicted. Three types of membrane pores were categorized: CH-1-*Pore A*, CH-1-*Pore B* and CH-1-*Pore C*. We found that the surface structures of CH-1-*Pore B* and CH-1-*Pore C* were smoother than that of CH-1-*Pore A* (Table 1). CH-1-*Pore C* had the largest pore opening among the three. Mean height of CH-1-*Pore A* was larger than the ones of CH-1-*Pore B* and CH-1-*Pore C*.

S. marcescens is a Gram-negative bacillus bacterium whose cell envelope consists of inner membrane (IM, or cytoplasmic membrane) and outer membrane (OM) [23]. These two layers form barriers to translocation of substances. Therefore, transport of substances into or out of the cell requires selective proteins [24]. These membrane proteins are critical to secreting proteins such as toxins and proteases, which is driven by inner membrane ATP-binding cassette (ABC) transporter. Membrane proteins are also central to discharging antibiotics, heavy metals and dyes, which occurs via inner proton antiporter [25]. Transports of the substances that occurs across the outer membrane are usually through diffusion following an ion concentration gradient. Active transport across the OM is possible by interacting with energized proteins of the IM.

The OM of *S. marcescens* is formed by lipid bilayer, which consists of proteins, phospholipids, and lipopolysaccharide [2]. In our study,

high-resolution images of the AFM showed that each type of pore has distinguished spatial arrangement of transmembrane subunits (protrusions). These protrusions might be constructed of lipopolysaccharides and proteins, such as porin proteins, specific channel-forming proteins and high-affinity receptors located on the outer membrane of *S. marcescens* CH-1 [26,27]. Using the AFM technique to analyze the membrane pore of *S. marcescens* cells, we observed that CH-1-*Pore A* had six to eight integral membrane subunits, which coincides with the voltage-gated potassium channel with six to eight integral membrane subunits arranged like the staves of a barrel around a central ion conduction pore [28, 29, 30, 31]. This is also likely to be part of efflux pump such as the ABC transporter that was found on *Serratia marcescens* [32]. In addition, we found that the structural arrangement of CH-1-*Pore B* (four-subunit one-pore doughnut-shaped) is in agreement with that of a prokaryotic voltage-gated potassium [15, 33] or canonical voltage-gated sodium channel [11] which has four subunits constituting a doughnut-shaped structure including the central hole. The four transmembrane structures of CH-1-*Pore B* were also possible to be part of small multidrug resistance efflux pumps that is composed of four transmembrane domains that span the cell membrane [34]. Finally, the two-subunit one-pore (inverted teepee-shaped) structure of CH-1-*Pore C* was similar to that of a prokaryotic inwardly rectifying potassium channel [35, 36, 37] which has been shown to contain two transmembrane segments and a pore loop in between.

In the AFM analysis, the topographic images of the cell were gathered by scanning the surfaces with mechanical probe (cantilever). The cantilever was brought into proximity of the surfaces, and was bended by the forces between the tip and sample surface. Therefore, AFM allows direct measurements of the pore dimensions [38]. Atomic resolution is achievable in AFM when measuring physically hard samples. However, the maximum resolution is in the order of 5 nm in the lateral and 0.5 nm in the vertical direction when measuring the softer biological samples [38, 39]. In this study, the diameter of the doughnut-like structure was possibly overestimated to a certain (as yet unknown) extent because of these technical reasons (AFM tip convolution). Moreover, the minimal diameter of the channel may be underestimated due to the intrinsic diameter of the tip. Consequently, the pore may exhibit a funnel-like profile with the narrower internal canal than measured. In addition to the artifacts caused by AFM tip and cantilever, preparation process can also contributed to the measured roughness. For example, samples might be dehydrated during the measurement that caused wrinkles on cell surfaces. The washing and re-suspend process might also introduced impurity on the samples.

In conclusion, this study represents the first direct characterization of the surface ultrastructure of the membrane pores of *Serratia marcescens* CH-1 cells at the nanometer scale and offers new prospects for mapping membrane pores of intact prokaryotic cells. We have obtained AFM images of three types of membrane pores of intact *S. marcescens* cells under physiological conditions and have shown some differences in surface structures. Topographic information of membrane pores obtained in this work will provide additional information to electrophysiological or X-ray structural data. Future experiments will focus on the specific recognitions of various membrane pores and the import and export processes that involve. These experiments will include but not limited to the use of atomic force microscopy combined with other variance of microscopies that provide high resolution and additional information. Examples of these microscopies include total internal refraction fluorescent microscopy, confocal microscopy, and scanning/transmitting electron microscopy. The knowledge of the structure will hopefully help the understanding of the export and import of substrates such as proteins and drugs, which might benefit the comprehension of drug resistance and the development of vaccine.

Declarations

Author contribution statement

Yu-Chun Lin: Conceived and designed the experiments; Performed the experiments; Analyzed and interpreted the data; Wrote the paper.

Cheng Huang: Conceived and designed the experiments; Performed the experiments; Analyzed and interpreted the data.

Hsin-Chih Lai: Conceived and designed the experiments; Analyzed and interpreted the data; Contributed reagents, materials, analysis tools or data.

Funding statement

This work was supported by research grant MOST 104-2320-B-077-003- and MOST 106-2320-B-010-038- from the Ministry of Science and Technology, Taiwan.

Competing interest statement

The authors declare no conflict of interest.

Additional information

No additional information is available for this paper.

Acknowledgements

The authors would like to thank Prof. Shiming Lin for his advices of AFM.

References

[1] World Health Organization (Ed.), Antimicrobial Resistance: Global Report on Surveillance, World Health Organization, Geneva, Switzerland, 2014.
[2] A. Hejazi, F.R. Falkiner, Serratia marcescens, J. Med. Microbiol. 46 (1997) 903–912.
[3] G. Binnig, C.F. Quate, Ch. Gerber, Atomic force microscope, Phys. Rev. Lett. 56 (1986) 930–933.
[4] M. Radmacher, R. Tillamnn, M. Fritz, H. Gaub, From molecules to cells: imaging soft samples with the atomic force microscope, Science 257 (1992) 1900–1905.
[5] H.-J. Butt, E.K. Wolff, S.A.C. Gould, B. Dixon Northern, C.M. Peterson, P.K. Hansma, Imaging cells with the atomic force microscope, J. Struct. Biol. 105 (1990) 54–61.
[6] H.J. Butt, K. Seifert, E. Bamberg, Imaging molecular defects in alkanethiol monolayers with an atomic force microscope, J. Phys. Chem. 97 (1993) 7316–7320.
[7] K. Miura, Y. Shukuya, Comparison between atomic force microscopic images of ionic crystal surfaces in air and in dry argon, Jpn. J. Appl. Phys. 32 (1993) 4752–4753.
[8] G. Liu, M.B. Salmeron, Reversible displacement of chemisorbed n-alkanethiol molecules on Au(111) surface: an atomic force microscopy study, Langmuir 10 (1994) 367–370.
[9] S. Xu, P.E. Laibinis, G. Liu, Accelerating the kinetics of Thiol self-assembly on GoldA spatial confinement effect, J. Am. Chem. Soc. 120 (1998) 9356–9361.
[10] L. Stehno-Bittel, C. Perez-Terzic, A. Luckhoff, D.E. Clapham, Nuclear ion channels and regulation of the nuclear pore, Soc. Gen. Physiol. Ser. 51 (1996) 195–207.
[11] D. Ren, A prokaryotic voltage-gated sodium channel, Science 294 (2001) 2372–2375.
[12] N. Armstrong, Y. Sun, G.-Q. Chen, E. Gouaux, Structure of a glutamate-receptor ligand-binding core in complex with kainate, Nature 395 (1998) 913–917.
[13] R. Milkman, An Escherichia coli homologue of eukaryotic potassium channel proteins, Proc. Natl. Acad. Sci. 91 (1994) 3510–3514.
[14] H. Schrempf, O. Schmidt, R. Kümmerlen, S. Hinnah, D. Müller, M. Betzler, T. Steinkamp, R. Wagner, A prokaryotic potassium ion channel with two predicted transmembrane segments from Streptomyces lividans, EMBO J. 14 (1995) 5170–5178.
[15] Y. Jiang, A. Lee, J. Chen, M. Cadene, B.T. Chait, R. MacKinnon, The open pore conformation of potassium channels, Nature 417 (2002) 523–526.
[16] M. Maduke, D.J. Pheasant, C. Miller, High-level expression, functional reconstitution, and quaternary structure of a prokaryotic clc-type chloride channel, J. Gen. Physiol. 114 (1999) 713–722.
[17] R. Iyer, T.M. Iverson, A. Accardi, C. Miller, A biological role for prokaryotic ClC chloride channels, Nature 419 (2002) 715–718.

[18] R. Dutzler, E.B. Campbell, M. Cadene, B.T. Chait, R. MacKinnon, X-ray structure of a ClC chloride channel at 3.0 Å reveals the molecular basis of anion selectivity, Nature 415 (2002) 287–294.
[19] C. Andersen, Channel-tunnels: outer membrane components of type I secretion systems and multidrug efflux pumps of Gram-negative bacteria, Rev. Physiol. Biochem. Pharmacol. 147 (2003) 122–165.
[20] Membrane channels, in: Cell Biology, Elsevier, 2017, pp. 261–284.
[21] K. Matsushita, J. Uchiyama, S. Kato, T. Ujihara, H. Hoshiba, S. Sugihara, A. Muraoka, H. Wakiguchi, S. Matsuzaki, Morphological and genetic analysis of three bacteriophages of *Serratia marcescens* isolated from environmental water, FEMS Microbiol. Lett. 291 (2009) 201–208.
[22] A. Franco-Obregón, H. Wang, D.E. Clapham, Distinct ion channel classes are expressed on the outer nuclear envelope of T- and B-lymphocyte cell lines, Biophys. J. 79 (2000) 202–214.
[23] F. Duong, J. Eichler, A. Price, M. Rice Leonard, W. Wickner, Biogenesis of the gram-negative bacterial envelope, Cell 91 (1997) 567–573.
[24] H. Nikaido, M. Vaara, Molecular basis of bacterial outer membrane permeability, Microbiol. Rev. 49 (1985) 1–32.
[25] M.H. Saier, A functional-phylogenetic classification system for transmembrane solute transporters, Microbiol. Mol. Biol. Rev. 64 (2000) 354–411.
[26] T. Matsuyama, A. Bhasin, R.M. Harshey, Mutational analysis of flagellum-independent surface spreading of Serratia marcescens 274 on a low-agar medium, J. Bacteriol. 177 (1995) 987–991.
[27] U. Ehrenhöfer, The atomic force microscope detects atp-sensitive protein clusters in the plasma membrane of transformed mdck cells, Cell Biol. Int. 21 (1997) 737–746.
[28] C. Parra-Lopez, R. Lin, A. Aspedon, E.A. Groisman, A Salmonella protein that is required for resistance to antimicrobial peptides and transport of potassium, EMBO J. 13 (1994) 3964–3972.
[29] R. MacKinnon, Pore loops: an emerging theme in ion channel structure, Neuron 14 (1995) 889–892.
[30] E.T. Buurman, K.-T. Kim, W. Epstein, Genetic evidence for two sequentially occupied K + binding sites in the kdp transport ATPase, J. Biol. Chem. 270 (1995) 6678–6685.
[31] L.Y. Jan, Y.N. Jan, Cloned potassium channels from eukaryotes and prokaryotes, Annu. Rev. Neurosci. 20 (1997) 91–123.
[32] T. Matsuo, J. Chen, Y. Minato, W. Ogawa, T. Mizushima, T. Kuroda, T. Tsuchiya, SmdAB, a heterodimeric ABC-type multidrug efflux pump, in Serratia marcescens, J. Bacteriol. 190 (2008) 648–654.
[33] D. Ungar, A. Barth, W. Haase, A. Kaunzinger, E. Lewitzki, T. Ruiz, H. Reiländer, H. Michel, Analysis of a putative voltage-gated prokaryotic potassium channel, Eur. J. Biochem. 268 (2001) 5386–5396.
[34] Y. Minato, F. Shahcheraghi, W. Ogawa, T. Kuroda, T. Tsuchiya, Functional gene cloning and characterization of the SsmE multidrug efflux pump from Serratia marcescens, Biol. Pharm. Bull. 31 (2008) 516–519.
[35] K.A. Ketchum, W.J. Joiner, A.J. Sellers, L.K. Kaczmarek, S.A.N. Goldstein, A new family of outwardly rectifying potassium channel proteins with two pore domains in tandem, Nature 376 (1995) 690–695.
[36] X.L. Zhou, B. Vaillant, S.H. Loukin, C. Kung, Y. Saimi, YKC1 encodes the depolarization-activated K+ channel in the plasma membrane of yeast, FEBS Lett. 373 (1995) 170–176.
[37] D. Guo, Y. Ramu, A.M. Klem, Z. Lu, Mechanism of rectification in inward-rectifier K + channels, J. Gen. Physiol. 121 (2003) 261–276.
[38] H. Oberleithner, E. Brinckmann, A. Schwab, G. Krohne, Imaging nuclear pores of aldosterone-sensitive kidney cells by atomic force microscopy, Proc. Natl. Acad. Sci. 91 (1994) 9784–9788.
[39] R.M. Henderson, S. Schneider, Q. Li, D. Hornby, S.J. White, H. Oberleithner, Imaging ROMK1 inwardly rectifying ATP-sensitive K+ channel protein using atomic force microscopy, Proc. Natl. Acad. Sci. 93 (1996) 8756–8760.